1st International Symposium on Laser Ultrasonics: Science, Technology and Applications
July 16-18 2008, Montreal, Canada

Fourier Domain Reconstruction Methods in Laser Ultrasonics and Photoacoustic Imaging

Peter BURGHOLZER [1], Thomas BERER [1], Bernhard REITINGER [1],
Robert NUSTER [2], Günther PALTAUF [2]

[1] Department of Sensors, Upper Austrian Research, Hafenstrasse 47-51, A-4020 Linz, Austria,
e-mail: Peter.Burgholzer@uar.at
[2] Karl-Franzens-University, A-8010 Graz, Austria

Abstract
Laser-ultrasonics as well as photoacoustic imaging use optically generated acoustic waves detected at the sample surface to image its interior. In laser-ultrasonics, a laser pulse is absorbed at the sample surface generating an ultrasound pulse that propagates into the sample, is reflected at internal structures, and is detected at the surface. In photoacoustic imaging, the source of the ultrasound wave is the investigated structure inside of an optical semitransparent sample itself. The goal in photoacoustic imaging is to recover the spatial distribution of absorbed energy density inside the sample from the acoustic pressure signals measured outside the sample (photoacoustic inverse problem). Fourier reconstruction is based on the decomposition into plane waves and is a fast and efficient method used in photoacoustic imaging. Interpolation is needed when signal Fourier components are mapped to source Fourier components. We have shown that the synthetic aperture focusing technique (SAFT) in frequency domain, which needs no interpolation, and the Fourier reconstruction method are mathematically equivalent if the step size of the spatial discretization goes to zero. Both imaging methods are compared using simulated data and measurement data acquired with our interferometer set-up.
Keywords: Laser ultrasound, photoacoustic imaging, frequency domain, Fourier reconstruction, synthetic aperture focusing technique (SAFT)

1. Introduction

Depending on where the conversion of optical into acoustic energy takes place, photoacoustic and laser ultrasound imaging modalities are distinguished. In Photoacoustic Imaging the source of ultrasound waves is the investigated structure inside of an optical semitransparent sample itself. The waves are generated by heating of light-absorbing structures within the object after illumination with a short laser pulse. If the laser pulse duration is shorter than the period of time that an acoustic wave needs to traverse such an absorbing structure (“stress confinement”) and if the thermal conductivity can be neglected during pulse time (“thermal confinement”), the thermal expansion leads to an efficient generation of a sound wave. This wave carries information about size, location and optical properties of the structure to the surface of the object where it is detected by broadband acoustic detectors. As described in the Introduction, for short laser pulses thermal waves can be neglected and only acoustic waves are used for imaging. This technique has been intensively investigated in the recent years [1].

The success of photoacoustic methods in biomedical imaging is based on the high optical contrast of some tissue constituents, such as blood vessels, compared to the surrounding tissue. Due to the strong light scattering in tissue, purely optical methods can only generate high resolution images of tissue to a depth where the light becomes diffuse (the diffusion length). Photoacoustic Imaging, on the other hand, uses the

coupling of the diffusely distributed optical energy into ultrasound waves, which propagate with only minimal scattering and allows therefore the generation of high contrast and high resolution images from areas beyond the light diffusion length.

Two modes of image formation exist in Photoacoustic Imaging, depending on the characteristics of the ultrasound detectors. Unfocused detectors with wide acceptance angle measuring signals from different directions around the object are used to reconstruct images with tomographic algorithms (PAT) or a focused detector is scanned across the surface of the object and the received signals are treated similar to amplitude scans in conventional ultrasound imaging (PAM).

In Laser Ultrasonics, a laser pulse is absorbed at the surface of the sample under investigation generating an ultrasound pulse that propagates into the sample. Waves reflected at structures with acoustic mismatch to the surrounding material or waves passing the sample are measured e.g. with a piezoelectric detector or by utilizing an optical, usually interferometric, technique. This method is therefore closely related to conventional ultrasound imaging, but takes advantage of the broad bandwidth of laser-generated ultrasound waves. Because objects can be inspected completely contact-free, the laser ultrasound technique has found widespread applications in materials testing. It has been suggested to modify the laser ultrasound technique for low absorbing samples by using an absorbing target near the tissue surface for ultrasound generation [2,3].

Table 1. Photoacoustic Imaging versus Laser Ultrasonics

	Optical absorption of sample	Acoustic impedance of sample
Photoacoustic Imaging	Varying absorption coefficient determines contrast	Assumed to be constant (at least in most publications)
Laser Ultrasonics	High absorption, therefore acoustic wave is generated at the sample surface	Contrast is determined by the varying acoustic impedance

In Photoacoustic Imaging it is assumed that the acoustic wave is generated inside the sample by thermoelastic expansion. In Laser Ultrasonics it is assumed that the pulse of electromagnetic radiation is absorbed at the surface of the sample and imaging is performed in pulse-echo mode like in conventional ultrasound imaging. The propagation of this acoustic wave will be influenced by acoustic heterogeneities, e.g. reflection on interfaces in the sample. Photoacoustic Imaging and Laser Ultrasonics are two special cases in this generalized frame (see Table 1). The information gained by both methods is complementary [4,5,6] and thus the combination is more accurate than using just one method.

2. Frequency domain and F-SAFT reconstruction

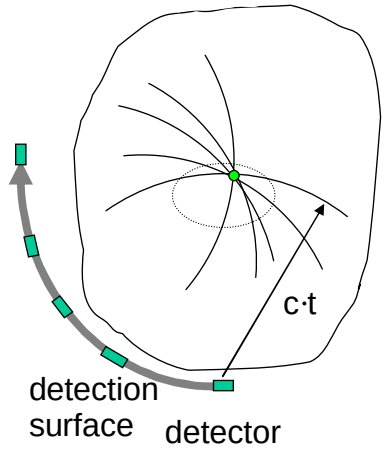

Figure 1. The detection surface is the surface formed by the receiver array of point like detectors or the surface over which a single receiver is scanned during signal acquisition.

A point like detector measures signals from all parts of the illuminated volume. The measured pressure signal at the detector at given time t is the integral over the surface of a sphere with radius ct if the sound velocity c is constant. The detection surface is the surface formed by the receiver array or the surface over which a single receiver is scanned during signal acquisition (Figure 1). For image reconstruction tomographical methods like spherical back-projection can be used. In the case of point like detectors, only for spherical, cylindrical, and planar detection surfaces exact inversion formulas have been reported: either in the frequency-domain [7,8,9,10] or in the time-domain [11,12,13].

Short laser pulses absorbed in a semitransparent object generate an initial pressure distribution $p_0(\mathbf{r}) = \Gamma \cdot W(\mathbf{r})$ proportional to the volumetric density $W(\mathbf{r})$ of the locally absorbed electromagnetic energy and the Grüneisen-parameter Γ. The induced pressure field at position $\mathbf{r}$ and time t is denoted by $p(\mathbf{r},t)$ and solves the inhomogeneous wave equation with a temporal Dirac delta function as source term [14]:

$$\left(\frac{\partial^2}{\partial t^2} - c^2\Delta\right) p(\mathbf{r},t) = \frac{\partial}{\partial t} p_0(\mathbf{r}) \cdot \delta(t) \tag{1}$$

where Δ is the Laplacian operator with respect to the $\mathbf{r}$ coordinates and c is the sound velocity. The inverse photoacoustic problem is to reconstruct the initial pressure distribution p_0 from a set of data $p(\mathbf{r}_S,t)$ measured with detectors at positions $\mathbf{r}_S$ on a detection surface S outside the object (Figure 1). The forward problem, the calculation of the pressure wave from the initial pressure distribution, can be solved using the Green's function [15] in free space leading to the Poisson integral

$$p(\mathbf{r}_S,t) = \frac{1}{4\pi c}\frac{\partial}{\partial t}\int_{|\mathbf{r}_S-\mathbf{r}|=ct} \frac{p_0(\mathbf{r})}{|\mathbf{r}_S-\mathbf{r}|} dS = \frac{1}{4\pi}\frac{\partial}{\partial t}\left(t \cdot \int_{|\mathbf{r}_S-\mathbf{r}|=ct} p_0(\mathbf{r}) d\Omega\right) \tag{2}$$

The first integral in Eq. (2) is a surface integral over a sphere with radius ct and center $\mathbf{r}_S$; it can be transformed into an integral over the solid angle, where $d\Omega = dS/(ct)^2$ is the solid angle element with respect to the center $\mathbf{r}_S$.

One image reconstruction method for a planar detection surface is the Fourier reconstruction, which is based on the decomposition into plane waves. It is a fast and efficient method used in photoacoustic imaging [14, 8]. In this section we show that this Fourier reconstruction and the synthetic aperture focusing technique (SAFT) in frequency domain (F-SAFT) are mathematically equivalent if the step size of the spatial discretization goes to zero. For simplicity the following equations are given in two dimensions (2D) – the 3D equations follow straight forward:

$$P(k_x,k_y)=\iint p_0(x,y)\,e^{-ik_x x}e^{-ik_y y}\,dxdy$$
$$p(x,y,t)=\frac{1}{(2\pi)^2}\iint P(k_x,k_y)\cos(\omega t)\,e^{ik_x x}e^{ik_y y}\,dk_x dk_y \qquad (3)$$
$$with\quad \omega = c\left|\vec{k}\right| = c\cdot\sqrt{k_x^2+k_y^2}$$

The measurements p(x,y=const.,t) at a line with constant y can be spatially Fourier transformed (variable x) and Cosinus transformed in time – this gives the auxiliary function $A(k_x,x,\omega)$:

$$A(k_x,y,\omega)\equiv\iint p(x,y,t)\cos(\omega t)\,e^{-ik_x x}e^{ik_y y}\,dxdt \qquad (4)$$

Using relation (3) the frequency ω can be replaced by the space frequency k_y, which leads to the desired Fourier transform $P(k_x, k_y)$:

$$P(k_x,k_y)=\frac{4c^2k_y}{c\cdot\sqrt{k_x^2+k_y^2}}e^{-iyk_y}A\left(k_x,y,c\cdot\sqrt{k_x^2+k_y^2}\right) \qquad (5)$$

Here we use that the initial pressure distribution is confined in the half space with y>0 and therefore $P(k_x,k_y<0)=0$.

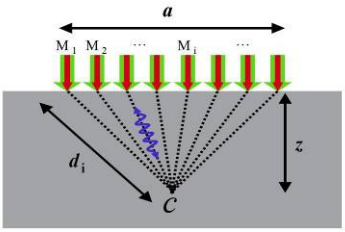

Figure 2. Schematic of the laser-ultrasonic inspection technique collecting a 2-D array of ultrasonic signals at the sample surface for its use with SAFT [16]. In Photoacoustic Imaging, the acoustic wave is directly generated at the inclusion C and has to propagate only one way from the inclusion to the detection point at the surface (M1, M2, …).

The frequency domain reconstruction is exact, if the scan length along the x-axis is infinite (e.g. the whole line y=0). Then from the measured p(x,y=0,t) the auxiliary function A can be calculated, eq. (5) can be used (with y=0) to calculate $P(k_x,k_y)$, and the inverse Fourier transform gives the initial pressure distribution p_0.

The F-SAFT algorithm has been applied to Laser Ultrasonics [16] and the imaging problem is the same as for Photoacoustic Imaging. Only the sound speed in Laser Ultrasonics has to be divided by a factor of two because the wave is generated at the sample surface, propagates to the image point (where e.g. the sample contains an inclusion), and again back to the surface, where it is detected. In Photoacoustic Imaging, the acoustic wave is directly generated at an inclusion and has to propagate only one way from the inclusion to the detection point at the surface (Figure 2). The F-SAFT algorithm can be also directly derived from eq. (5):

$$A(k_x,y,\omega)=e^{+iyk_y}A(k_x,y=0,\omega) \qquad (6)$$

The transformed field A is back-propagated to any depth y using eq. (6). Also the F-SAFT algorithm gives only an exact reconstruction if the scan length along the *x*-axis is infinite. Both reconstruction algorithms are sketched in Figure 3.

To test both reconstruction methods with a finite scan length and a finite number of detection points (N=300) we performed the following simulation. The source in this 2D simulation is a Gaussian shaped peak.

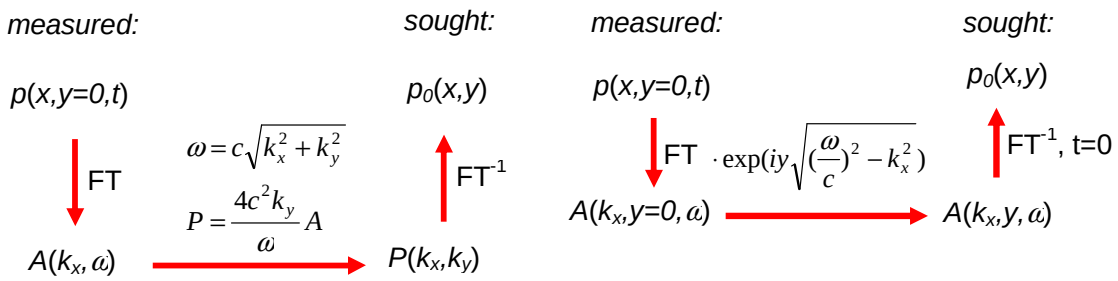

Figure 3. left: Frequency domain; right: F-SAFT reconstruction.

The reconstruction using the finite scan data along the *x*-axis is shown in Figure 4a and 4b together with the corresponding 2D spectrum in Figure 4c. It can be clearly seen that the resolution in *x* direction is worse than in *y* direction. This is a result of the missing information in frequency space, where a large wedge shaped area near the k_x axis contains no data.

(a)

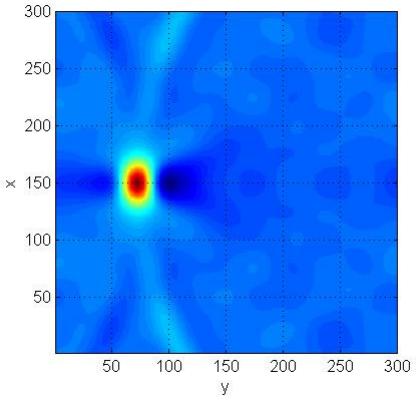

(b)

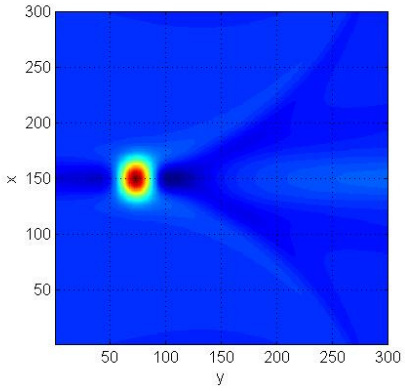

(c)

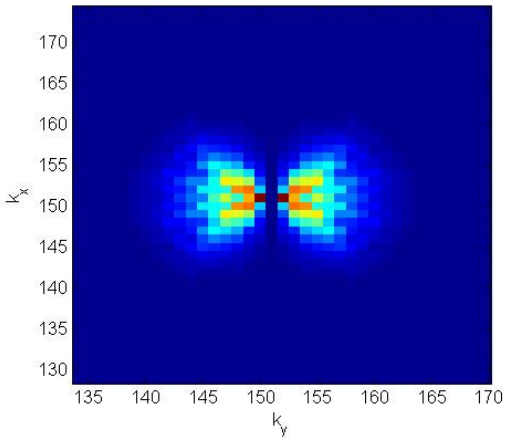

Figure 4. (a) Frequency domain, (b) F-SAFT reconstruction , (c) together with the corresponding 2D spectrum.

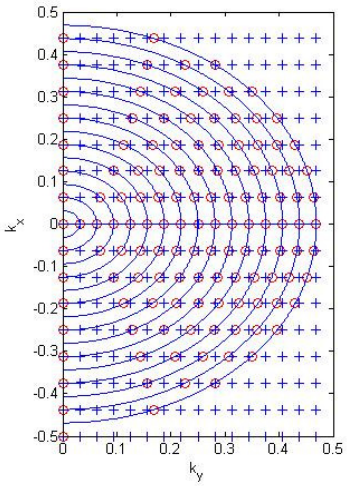

Figure 5. Frequency domain reconstruction: for discrete data points interpolation is needed when signal Fourier components are mapped to source Fourier components according to eq. (5).

For frequency-domain reconstruction with discrete data points interpolation is needed when signal Fourier components are mapped to source Fourier components according to eq. (5) (see Figure 5). This interpolation can be avoided using nonequidistant fast Fourier transform (NFFT) or the artifacts caused by this interpolation can be minimized using a truncated regularized inverse k-space interpolation, as recently shown by Jaeger et al. [17]. F-SAFT needs no such interpolation, therefore those artifacts are reduced. Therefore more calculation time is needed (inverse FT is needed for every depth y).

3. L – reconstruction

In order to fill the frequency space with the missing data either the scan line along the *x*-axis has to be extended considerably, or a second scan perpendicular to the first one, along the *y*-axis can be used. The reconstruction resulting from the second scan is shown in Figure 6c, its Fourier transform in Figure 6d.

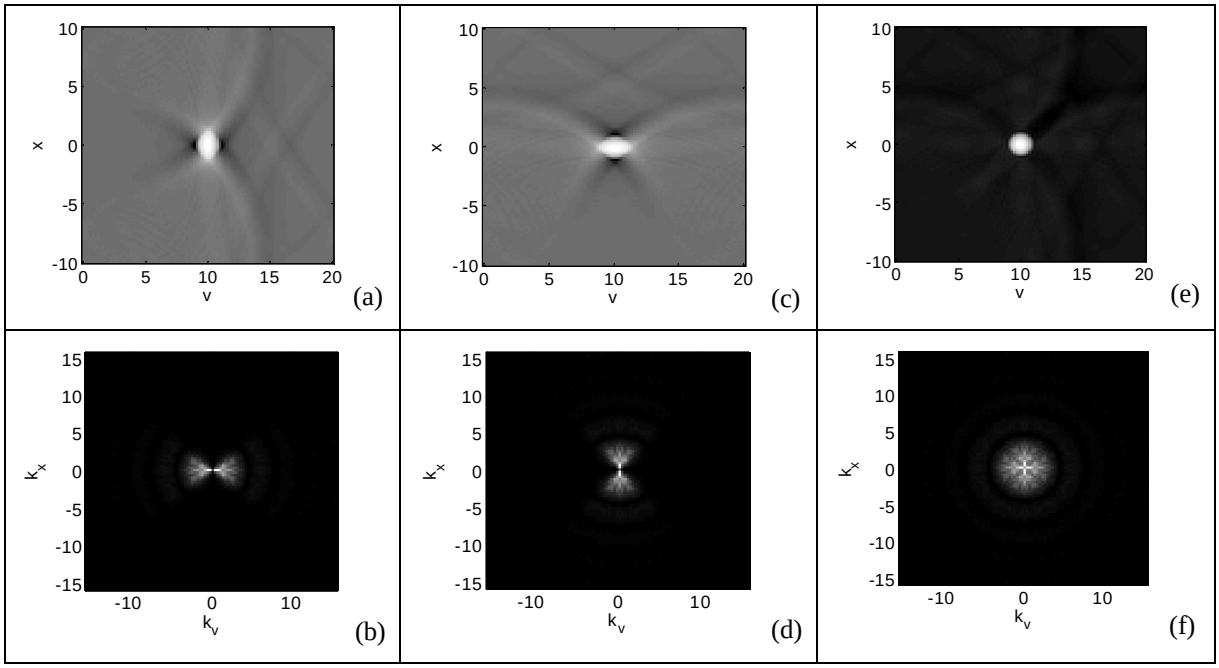

Figure 6. Simulated PAT: (a) Reconstruction using data in Fig. 4, (b) amplitude of the Fourier transform of the reconstructed image. (c) Reconstruction from a scan along the *y*-axis at $x = 0$, (d) corresponding Fourier transform. (e) L-reconstruction obtained by adding the images in (a) and (c). (f) Fourier transform of the L-reconstruction.

It can be seen that the information in frequency space of the two perpendicular scans is complementary. The simplest way to complete the data is therefore just to add the two Fourier transforms. This addition can be as well carried out in real space, resulting in the reconstruction that is seen in Figure 6e. The reconstructed image of the sphere has

equally good resolution in all directions. Moreover, the artifacts in the reconstructions of the individual scans, such as arcs outside the sphere and negative values (black areas in (a) and (c)), have cancelled out each other in the combined reconstruction. The improvement of the reconstruction is correlated with the filling of the frequency domain, as can be seen in Figure 6f. Because the motion of the detector line has the shape of an “L” we will refer to this algorithm as “L-reconstruction”.

4. Conclusions

Frequency domain and F-SAFT reconstruction both suffer from limited view. The simplest way to improve frequency domain and F-SAFT reconstruction was to add two images arising from two orthogonal linear scans. The rationale for this step was the observation that in frequency space the information of the two scans appeared to be complementary. Another obvious reason why the combined image must have higher quality is the larger detection view.

Acknowledgements

This work has been supported by the Austrian Science Fund (FWF), project P18172-N02 and project L418-N20.

References

1. M. H. Xu and L. H. V. Wang, "Photoacoustic Imaging in Biomedicine," Review of Scientific Instruments 77, 041101-041122 (2006).
2. J. D. Hamilton and M. O'Donnel, "High frequency ultrasound imaging with optical arrays," IEEE Trans. Ultrason., Ferroelect., Freq. Contr. 45, 216-235 (1998).
3. A. Meyer, S. Gspan, S. Bernet, and M. Ritsch-Marte, "Binary optoacoustic holography with a spatial light modulator," J. Appl. Phys. 96, 5886-5891 (2004).
4. J. J. Niederhauser, M. Jaeger, R. Lemor, P. Weber, and M. Frenz, "Combined Ultrasound and Optoacoustic System for Real-Time High-Contrast Vascular Imaging in Vivo," IEEE Trans. Med. Imag. 24, 436-440 (2005).
5. Y. G. Zeng, D. Xing, Y. Wang, B. Z. Yin, and Q. Chen, "Photoacoustic and ultrasonic coimage with a linear transducer array," Optics Letters 29, 1760-1762 (2004).
6. X. Jin and L.V. Wang, “Correction of the effects of acoustic heterogeneity on thermoacoustic tomography using transmission ultrasound tomography”, Proc SPIE 60860W (2006).
7. S. J. Norton and M. Linzer, IEEE Transactions on Biomedical Engineering 28, 202 (1981).
8. K. P. Köstli, M. Frenz, H. Bebie, and H. P. Weber, Phys. in Med. and Biology 46, 1863 (2001).
9. Y. Xu, D. Feng, and L.-H. Wang, “Exact Frequency-Domain Reconstruction for Thermoacoustic Tomography - I: Planar Geometry”, IEEE Transactions on Medical Imaging 21, 823 (2002).
10. Y. Xu, M. Xu, and L.-H. Wang, “Exact Frequency-Domain Reconstruction for Thermoacoustic Tomography - II: Cylindrical Geometry”, IEEE Transactions on Medical Imaging, IEEE Transactions on Medical Imaging 21, 829 (2002).

11. M. Xu and L.-H. Wang, IEEE Transactions on Medical Imaging 21, 814 (2002).
12. D. Finch, S. Patch, and Rakesh, SIAM J. Math. Anal. 35, 1213 (2004).
13. M. Xu and L.-H. Wang, Physical Review E 71, 016706 (2005).
14. K. P. Köstli, D. Frauchinger, J. Niederhauser, G. Paltauf, H. Weber, and M. Frenz, IEEE, Journal on selected Topics in Quantum Electronics 7, 918 (2001).
15. P. M. Morse and H. Feshbach, "Methods of theoretical physics", McGraw-Hill, New York (1953).
16. D. Levesque, A. Blouin, C. Neron, and J.-P. Monchalin, "Performance of laser-ultrasonic F-SAFT imaging", Ultrasonics 40, 1057-1063 (2002).
17. M. Jaeger, S. Schüpbach, A. Gertsch, M. Kitz, and Martin Frenz, „Fourier reconstruction in optoacoustic imaging using truncated regularized inverse k-space interpolation", Inverse Problems 23, S51-S63 (2007).